

# Thermal instability in drawing viscous threads

By JONATHAN J. WYLIE<sup>1</sup>, HUAXIONG HUANG<sup>2</sup>  
AND ROBERT M. MIURA<sup>3</sup>

<sup>1</sup>Department of Mathematics, City University of Hong Kong, Kowloon, Hong Kong

<sup>2</sup>Department Mathematics and Statistics, York University, Toronto, Ontario, Canada M3J 1P3

<sup>3</sup>Department of Mathematical Sciences, New Jersey Institute of Technology, Newark, NJ 07102, USA.

(Received January 2006 and in revised form ??)

We consider the stretching of a thin viscous thread, whose viscosity depends on temperature, that is heated by a radiative heat source. The thread is fed into an apparatus with a fixed speed and stretched by imposing a higher pulling speed at a fixed downstream location. We show that thermal effects lead to the surprising result that steady states exist for which the force required to stretch the thread can decrease when the pulling speed is increased. By considering the nature of the solutions, we show that a simple physical mechanism underlies this counterintuitive behavior. We study the stability of steady-state solutions and show that a complicated sequence of bifurcations can arise. In particular, both oscillatory and non-oscillatory instabilities can occur in small isolated windows of the imposed pulling speed.

---

## 1. Introduction

Stretching viscous fluids into long thin threads is important in a broad range of applications. Examples include the use of polymeric materials and glass to produce textiles and fiber optics (Denn 1980 and Fitt *et al.* 2001). The production process often requires high temperatures to facilitate stretching with moderate forces. The viscosity of the materials that are typically used can vary dramatically with temperature. Therefore, the resulting thermal gradients can be significant, leading to large gradients in the viscosity of the thread. In some cases, external heating is applied to parts of the thread to prevent other localized regions of high viscosity from developing.

Fiber stretching in the isothermal case has been widely studied (see, for example, Denn 1980, Dewynne *et al.* 1992, Cummings & Howell 1999). If the draw ratio, i.e., ratio of the speed at which the fiber exits the device to that at which it enters, exceeds a critical value then the process is subject to an oscillatory instability known as draw resonance. A number of authors have considered how thermal effects modify thread drawing (Shah & Pearson 1972a,b, Pearson & Shah 1973, Yarin 1986, Gupta & Schultz 1998, and Forest & Zhou 2001). Thermal effects also have been considered in a number of experimental studies (Fisher & Denn 1977, Han & Apte 1979), but these have mostly focused on the use of cooling to suppress draw resonance. Matsumoto & Bogue (1978) conducted experiments in which temperature changes cause the material to experience a phase transition. They found that instability could arise that cannot be explained using a traditional draw resonance analysis. Blyler & Gieniewski (1980) have carried out experiments that consider external heating of the thread. They used a material whose

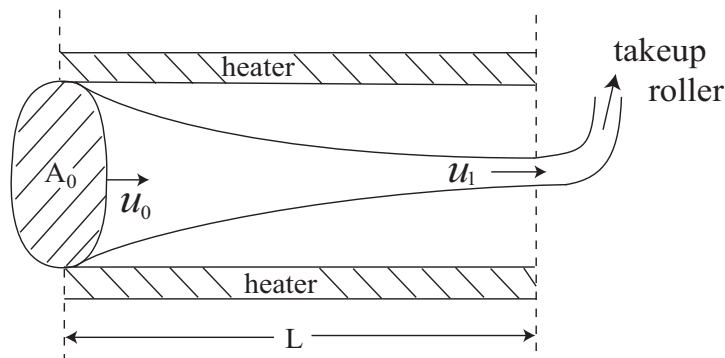


FIGURE 1. Fluid is fed in through a circular aperture of cross-sectional area  $A_0$  with speed  $u_0$  and temperature  $\theta_0$  and is drawn at a fixed speed  $u_1$  by a take-up roller that is a distance  $L$  from the aperture. The thread is heated while it is in the device.

viscosity varies abruptly with temperature and observed that the process is extremely sensitive to the axial temperature profile. They showed that a number of mechanisms can cause instability. Even at very low draw ratios they found that the drawing process became extremely sensitive to perturbations if the heating rate exceeded a critical value. Nevertheless, previous theoretical studies showed that the stability boundaries, frequency, and amplitude for the draw resonance instability are modified, but found no qualitatively different dynamics when compared to the isothermal case.

In contrast, we show that thermal effects can lead to fundamentally different dynamics. For example, rather than having a unique steady solution, multiple steady states can exist. For a range of draw ratios, steady states can exist in which an increase in the pulling speed leads to a decrease in the force required to pull the thread. We propose a mechanism that underlies this behavior and show that such solutions are always unstable. Nonunique solutions exist if the viscosity varies sufficiently abruptly with temperature and heating is strong enough to cause sufficiently large variations. In addition, if the viscosity varies sufficiently abruptly with temperature, there are other instabilities (both oscillatory and non-oscillatory) that occur in small isolated windows of the draw ratio. These isolated windows tend to occur near draw ratios for which multiple solutions exist.

## 2. Formulation

We consider a device that feeds an axisymmetric cylindrical thread of viscous fluid at a constant speed  $u_0$  and temperature  $\theta_0$  through an aperture with radius  $R_0$  and cross-sectional area  $A_0 = \pi R_0^2$  (Figure 1). At a distance  $L$  from the aperture, the thread is drawn out of the device at a fixed speed  $u_1$  by a receiving apparatus. The thread is exposed to radiative heat transfer as it passes through the device.

Assuming that the length to thickness aspect ratio of the thread is large and the temperature is radially uniform, one can use one-dimensional long-wave equations for the conservation of mass and momentum that have been developed by a number of authors, including Forest & Zhou (2001). In the following paragraphs, we will show that the assumption of radially uniform temperature is valid for typical parameter values. The equation for conservation of mass is given by

$$A_t + (uA)_x = 0 \quad (2.1)$$

where  $x$  is the distance along the thread measured from the aperture,  $t$  is the time,  $u(x, t)$

is the velocity of the thread, and  $A(x, t)$  is the cross-sectional area. Neglecting gravity, the momentum equation is given by

$$\rho A \left( \frac{\partial u}{\partial t} + u \frac{\partial u}{\partial x} \right) = \frac{\partial}{\partial x} \left( 3\mu(\theta)A \frac{\partial u}{\partial x} + \gamma \pi R \right) \quad (2.2)$$

where  $R(x, t)$  is the radius,  $\mu$  is the viscosity that depends only on the temperature  $\theta$ ,  $\rho$  is the density, and  $\gamma$  is the surface tension coefficient. The surface tension and density also may depend on temperature, but the relative magnitude of their variation is generally much weaker than that of the viscosity and so, for simplicity, we take them to be constant. In the long-wavelength limit, axial conduction can be neglected and the heat equation is given by

$$\theta_t + u\theta_x = \frac{k}{\rho c_p} \frac{1}{r} \frac{\partial}{\partial r} \left( r \frac{\partial \theta}{\partial r} \right) \quad (2.3)$$

where  $r$  is the axisymmetric radial position and  $c_p$  and  $k$  are the specific heat capacity and the thermal conductivity of the fluid, respectively. The radiative boundary condition is given by

$$-k \left. \frac{\partial \theta}{\partial r} \right|_{r=R} = \alpha k_b (\theta^4 - \theta_h^4) \quad (2.4)$$

where  $k_b$  is the Boltzmann constant,  $\alpha$  is the absorptivity, and  $\theta_h$  is the heater temperature.

The fluid speed, cross-sectional area, and temperature are specified at the input

$$u = u_0, \quad A = A_0, \quad \theta = \theta_0 \quad \text{at } x = 0, \quad (2.5)$$

and the speed is specified at the exit

$$u = u_1 \quad \text{at } x = L. \quad (2.6)$$

We also must specify the dependence of the viscosity on temperature. An exponential function is often used in modeling the viscosity of glass materials and polymers. However, this may not be an appropriate model for multicomponent melts in which phase transitions can give rise to abrupt changes in viscosity as the temperature varies. For example, in their thread drawing experiments, Blyler & Gieniewski (1980) used an  $\alpha$ -methyl styrene/silicone block compound whose viscosity is almost completely insensitive to temperature changes in the range 100–140°C but drops by an order of magnitude between 140°C and 180°C (see Figure 1 of their paper). Empirical data for the viscosity of soda-lime also shows abrupt changes in viscosity (Pyrex Glass Code 1987). In this case, the viscosity drops by a factor of approximately 1.5 between 900°C and 1100°C, but drops by a factor of approximately 25 between 1100°C and 1300°C. Other studies also have noted that polymer crystallization can lead to even more dramatic increases in viscosity (Vassilatos *et al.* 1985). These abrupt changes often are modeled using a step-function model (Whitehead & Helfrich 1991). We will show that the abruptness of viscosity changes plays an important role in characterizing the dynamics. For simplicity, we adopt a hyperbolic tangent function that varies between a viscosity value  $\mu_0$  at low temperatures and a viscosity  $\mu_0 M$  at high temperatures

$$\mu(\theta) = \mu_0 \left[ \frac{(1+M)}{2} - \frac{(1-M)}{2} \tanh \left( \frac{\theta - \theta_0 - \theta_a}{\theta_r} \right) \right] \quad (2.7)$$

where  $\mu_0$  is a reference value of the viscosity,  $M < 1$  is a viscosity contrast that determines the size of changes in viscosity,  $\theta_a$  is the temperature increase from the input temperature required to cause a significant drop in the viscosity, and  $\theta_r$  represents the temperature

range over which the rapid viscosity changes occur. This model gives sufficient flexibility to characterize the principal features of viscosity laws that are appropriate in many applications and allows us to easily vary both the absolute magnitude and abruptness of viscosity changes in a simple way. Over the finite range of temperatures that can occur in such applications, this model can provide a reasonable approximation to the important qualitative features of the exponential model, the step-function model, and the empirical data for soda-lime. More realistic viscosity functions yield qualitatively similar results. Although this law has a number of parameters, only two dimensionless groups play a significant role in determining the qualitative behavior of the system.

Typical parameter values used in glass pulling that are relevant to fiber optics are given in Fitt *et al.* (2001) and Huang *et al.* (2003). These are  $L = O(10^{-2})$  m,  $R_0 = O(10^{-4})$  m,  $u_0 = O(10^{-2})$  m/s,  $\rho = 2.23 \times 10^3$  kg/m<sup>3</sup>,  $c_p = 7.538 \times 10^2$  J/K/kg,  $k = 1.130$  W/m/K,  $k_b = 5.67 \times 10^{-8}$  W/m<sup>2</sup>/K<sup>4</sup>,  $\theta_h = 800$  K,  $\theta_a = 50$  K,  $\gamma = O(10^{-1})$  kg/s<sup>2</sup>,  $\alpha = 0.4$ , and  $\mu_0 = O(10^4)$  kg/m/s. We nondimensionalize the equations using the following scales:

$$u = u_0 u', \quad A = A_0 A', \quad x = L x', \quad t = L u_0^{-1} t', \quad \theta = \theta_0 + \theta_a \theta', \quad \mu(\theta) = \mu_0 \mu'(\theta').$$

After substitution into (2.1)–(2.4) and dropping the primes, we find that the equation of conservation of mass (2.1) is unchanged. The momentum equation becomes

$$Re \left( \frac{\partial u}{\partial t} + u \frac{\partial u}{\partial x} \right) = \frac{1}{A} \frac{\partial}{\partial x} \left( \mu A \frac{\partial u}{\partial x} + \lambda R \right) \quad (2.8)$$

where

$$Re = \frac{\rho u_0 L}{3\mu_0} = O(10^{-5}), \quad (2.9)$$

is the Reynolds number which represents the ratio of inertia forces to viscous forces, and

$$\lambda = \frac{\gamma L}{3\mu_0 u_0 R_0} = O(10^{-2}), \quad (2.10)$$

is the ratio of surface tension forces to the viscous force. Since  $Re$  and  $\lambda$  are typically small we will neglect inertia and surface tension. The heat equation becomes

$$Pe \left( \frac{\partial \theta}{\partial t} + u \frac{\partial \theta}{\partial x} \right) = \frac{1}{r} \frac{\partial}{\partial r} \left( r \frac{\partial \theta}{\partial r} \right) \quad (2.11)$$

where

$$Pe = \frac{\rho c_p u_0 R_0^2}{Lk} = O(10^{-2}) \quad (2.12)$$

is the transverse Peclet number which represents the ratio of heat advected along the thread to heat conducted across the thread. The radiative boundary condition becomes

$$\left. \frac{\partial \theta}{\partial r} \right|_{r=R} = Bi H(\theta) \quad (2.13)$$

where

$$Bi = \frac{\alpha k_b \theta_h^4 R_0}{k \theta_a} = O(10^{-2}), \quad (2.14)$$

is the Biot number. The dimensionless function  $H(\theta) = 1 - \theta_h^{-4}(\theta_0 + \theta_a \theta)^4$  represents the magnitude of the net heat flux that is absorbed when the temperature is  $\theta$ .

The dimensionless heater strength is given by

$$\mathcal{H} \equiv \frac{2\sqrt{\pi} Bi}{Pe} = \frac{2\sqrt{\pi} \alpha L k_b \theta_h^4}{\rho c_p \theta_a u_0 R_0} = O(1), \quad (2.15)$$

which can be thought of as the heat absorbed by a thread moving with constant speed  $u_0$  divided by the heat required to significantly change the viscosity. Small values of  $\mathcal{H}$  imply that the viscosity remains almost constant, and so the solution will be similar to the isothermal case. Large values of  $\mathcal{H}$  imply that significant viscosity gradients will occur in the thread.

We assume that both  $Bi$  and  $Pe$  are small in such a way that their ratio is  $O(1)$ . Assuming the temperature has an asymptotic expansion of the form

$$\theta = \Theta_0 + Bi\Theta_1 + \dots, \quad (2.16)$$

then substituting into (2.11) and (2.13) and collecting the terms to zeroth and first-order in  $Bi$  yields

$$\frac{1}{r} \frac{\partial}{\partial r} \left( r \frac{\partial \Theta_0}{\partial r} \right) = 0, \quad \text{with} \quad \left. \frac{\partial \Theta_0}{\partial r} \right|_{r=R} = 0 \quad (2.17)$$

and

$$\frac{1}{r} \frac{\partial}{\partial r} \left( r \frac{\partial \Theta_1}{\partial r} \right) = \frac{2\sqrt{\pi}}{\mathcal{H}} \left( \frac{\partial \Theta_0}{\partial t} + u \frac{\partial \Theta_0}{\partial x} \right) \quad \text{with} \quad \left. \frac{\partial \Theta_1}{\partial r} \right|_{r=R} = H(\Theta_0). \quad (2.18)$$

Equation (2.17) implies that at leading order  $\Theta_0$  is independent of  $r$ . Therefore, using (2.18), we see that  $\Theta_0$  satisfies

$$\frac{\partial \Theta_0}{\partial t} + u \frac{\partial \Theta_0}{\partial x} = \frac{\mathcal{H}H(\Theta_0)}{\sqrt{A}}. \quad (2.19)$$

For notational brevity, we use  $\theta$  to denote the leading order term,  $\Theta_0$ . Having neglected the inertial and surface tensions terms, we obtain the equations

$$A_t + (uA)_x = 0, \quad (2.20)$$

$$[\mu(\theta)Au_x]_x = 0, \quad (2.21)$$

$$\theta_t + u\theta_x = \mathcal{H}H(\theta)A^{-1/2}. \quad (2.22)$$

The dimensionless viscosity function is given by

$$\mu(\theta) = \frac{(1+M)}{2} - \frac{(1-M)}{2} \tanh[K(\theta-1)] \quad (2.23)$$

where  $K = \theta_a/\theta_r$  is a measure of the abruptness of the change in viscosity. The dimensionless entry and exit conditions are

$$u = 1, \quad A = 1, \quad \theta = 0 \quad \text{at} \quad x = 0 \quad \text{and} \quad u = D_r \quad \text{at} \quad x = 1, \quad (2.24)$$

respectively, where

$$D_r = \frac{u_1}{u_0} \quad (2.25)$$

is the draw ratio.

The momentum equation (2.21) can be integrated to yield

$$\mu(\theta)Au_x = 2\mathcal{F} \quad (2.26)$$

where  $\mathcal{F}$  is the dimensionless pulling force, which must be determined by the boundary conditions. For unsteady calculations,  $\mathcal{F}$  will depend on time, but in this paper, we will focus on steady states in which case  $\mathcal{F}$  will be a constant.

In practice, the heating term,  $H$ , may be slightly more complicated than the one we have used here depending on the design and location of the heater, see Huang *et al.* (2003). However, the approach we adopt in this paper can be applied to any heater design,

viscosity law, and heating parameters. To illustrate the underlying physical mechanisms that occur in thermal thread drawing, we will choose simple, but physically relevant functional forms. Specifically, we consider the case in which the heater is assumed to supply a constant heating rate along the length of the thread. For simplicity, we will assume that typical temperatures attained by the fluid are sufficiently lower than the heater temperature that  $\theta_h^4$  is significantly larger than  $\theta^4$ . This implies that the dimensionless heater profile is given by  $H(\theta) = 1$ . Inclusion of the full heating terms with realistic parameter values does not significantly modify the results.

### 3. Steady state solutions

We begin by seeking steady state solutions of (2.20), (2.22) and (2.26). The conservation of mass equation (2.20) and the entry conditions (2.24) yield

$$uA = 1. \quad (3.1)$$

We eliminate  $u$  from equations (2.22) and (2.26) to obtain

$$\mu(\theta) \frac{A_x}{A} = -2\mathcal{F} \quad (3.2)$$

and

$$\theta_x = \mathcal{H}A^{1/2}. \quad (3.3)$$

It is possible to obtain integrals of (3.2) and (3.3) and write the solution formally in terms of integrals of the viscosity function. However, for most viscosity laws, it is more convenient to integrate (3.2) and (3.3) using a standard Runge-Kutta technique. In actuality, the dimensionless pulling force is a function of the exogenous variables  $\mathcal{H}$  and  $D_r$ , but one can more easily generate plots by taking fixed values of  $\mathcal{H}$  and  $\mathcal{F}$  and finding the appropriate value of  $D_r$ . This can be done by numerically integrating from  $x = 0$  to  $x = 1$  and using the boundary conditions (2.24).

In Figure 2, we plot the dimensionless pulling force against the draw ratio for different dimensionless heating rates and an abruptly varying viscosity law (large  $K = 12$ ) with a large change in viscosity (small  $M = 0.1$ ). For  $\mathcal{H}$  below a critical value of approximately 1.43, the pulling force is a monotonically increasing function of the draw ratio. However, for a sufficiently large heating rate, the curve develops two fold points (labeled  $c$  and  $d$  for  $\mathcal{H} = 1.6$  in Figure 2), the force is no longer unique and there is a range of draw ratios over which three steady states can be found. We note that between the two fold points there are solutions for which the pulling force decreases as the draw ratio increases. For a wide range of parameters, three steady states was the maximum number that was observed.

We investigate this highly counterintuitive behavior and describe the simple physical mechanism underlying this phenomenon. We choose a draw ratio for which three possible solutions exist and note that the distinct solutions correspond to different pulling forces. In Figure 3, we plot the cross-sectional area and temperature for each of the three solutions as functions of  $x$ . We note that the velocity is given by  $u = A^{-1}$ .

We begin by noting that (3.2), can be rewritten to show how the rate at which the cross-sectional area decreases is determined by the force and the viscosity,

$$(\ln A)_x = -\frac{2\mathcal{F}}{\mu(\theta)}. \quad (3.4)$$

When the fluid enters the device, the temperature and, hence, the viscosity are the same for all three solutions. Therefore, from (3.4), the area decreases most slowly for the case with the smallest force. Conservation of mass (2.20) implies that the larger the area, the

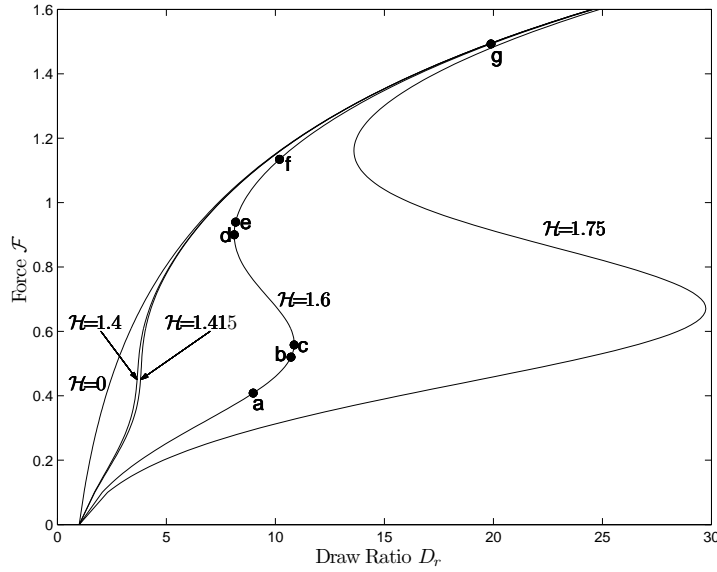


FIGURE 2. The dimensionless force  $\mathcal{F}$  as a function of the draw ratio  $D_r$  for different values of the heating rate  $\mathcal{H}$  with  $M = 0.1$  and  $K = 12$ . The points labeled  $a-g$  are included for easy comparison with the  $\mathcal{H}$  graph in Figure 6D which shows stability results.

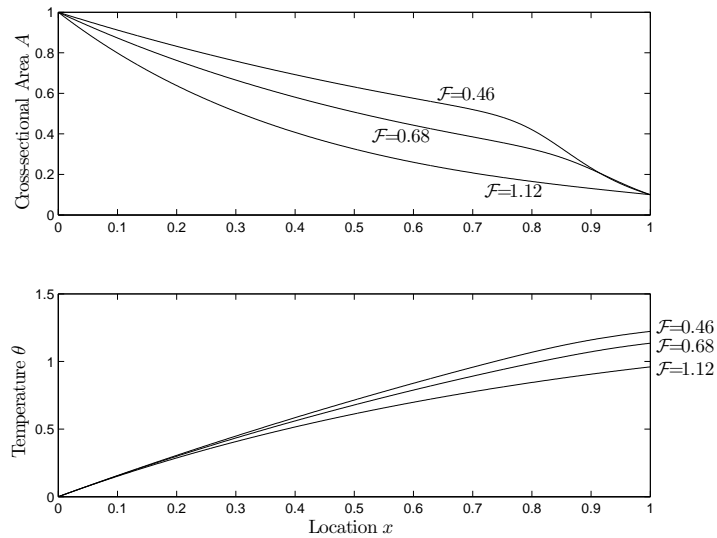


FIGURE 3. The cross-sectional area  $A$  and temperature  $\theta$  are plotted against the location  $x$  for the three solutions that exist for a draw ratio  $D_r = 10$  and  $\mathcal{H} = 1.6$ . The curves are identified by the three dimensionless force values  $\mathcal{F}$  that result for the given draw ratio .

slower the speed of the fluid thread. Hence, the thread with the smallest force moves more slowly, is exposed to radiative heating for a longer time, and will attain a higher temperature near the exit. This higher temperature implies that the viscosity near the exit will be smaller, and from (3.4), the thread will thin more rapidly there. If the decrease in the viscosity is large enough, then the thread with the smallest force can dramatically speed up (and thin) in the region near the exit and result in a thread that has the same

speed (and area) at the exit as the other two cases. A similar argument explains the existence of the solution with the intermediate pulling force.

In order to obtain these non-unique steady states for fixed draw ratio, it is important that the viscosity in the thread varies sufficiently abruptly with temperature (large  $K$ ) and has a sufficiently large change in viscosity (small  $M$ ). We therefore consider the large  $K$  asymptotics of the solution. Using the viscosity function (2.7), one can obtain an analytic expression for the first integral of (3.2)-(3.3), given by

$$A^{\frac{1}{2}} = 1 - \frac{\mathcal{F}}{\mathcal{H}} \left[ \theta + \frac{1-M}{2MK} \ln \left( \frac{1 + Me^{2K(\theta-1)}}{1 + Me^{-2K}} \right) \right]. \quad (3.5)$$

Hence (3.3) becomes

$$\theta_x = \mathcal{H} - \mathcal{F} \left[ \theta + \frac{1-M}{2MK} \ln \left( \frac{1 + Me^{2K(\theta-1)}}{1 + Me^{-2K}} \right) \right]. \quad (3.6)$$

When  $K$  is large, this equation can be approximated as

$$\theta_x = \mathcal{H} - \mathcal{F}\theta \quad (3.7)$$

for  $\theta < 1$  and

$$\theta_x = \mathcal{H} - \frac{\mathcal{F}}{M}(\theta + M - 1) \quad (3.8)$$

for  $\theta > 1$ . When  $\theta = 1 + O(K^{-1})$ , there is a transition layer of width of the order  $1/K$ . This transition layer is passive in the sense that the jump in  $\theta$  across the layer is zero at leading order.

Ignoring the passive transition layer, the leading order solution is given by

$$u = A^{-1} = \begin{cases} \exp[2\mathcal{F}x] & \text{if } x < \frac{1}{\mathcal{F}} \ln \left( \frac{\mathcal{H}}{\mathcal{H} - \mathcal{F}} \right) \\ \exp \left[ \frac{2\mathcal{F}x}{M} + \frac{2(M-1)}{M} \ln \left( \frac{\mathcal{H}}{\mathcal{H} - \mathcal{F}} \right) \right] & \text{if } x > \frac{1}{\mathcal{F}} \ln \left( \frac{\mathcal{H}}{\mathcal{H} - \mathcal{F}} \right) \end{cases}, \quad (3.9)$$

and

$$\theta = \begin{cases} \frac{\mathcal{H}}{\mathcal{F}}(1 - e^{-\mathcal{F}x}) & \text{if } x < \frac{1}{\mathcal{F}} \ln \left( \frac{\mathcal{H}}{\mathcal{H} - \mathcal{F}} \right) \\ 1 + \frac{M(\mathcal{H} - \mathcal{F})}{\mathcal{F}} \left[ 1 - \left( \frac{\mathcal{H}}{\mathcal{H} - \mathcal{F}} \right)^{1/M} e^{-\mathcal{F}x/M} \right] & \text{if } x > \frac{1}{\mathcal{F}} \ln \left( \frac{\mathcal{H}}{\mathcal{H} - \mathcal{F}} \right) \end{cases}. \quad (3.10)$$

By substituting  $x = 1$  into (3.9), we obtain the value of the draw ratio,  $D_r = u(1)$  as a function of  $\mathcal{F}$

$$D_r = \begin{cases} \exp[2\mathcal{F}] & \text{if } \mathcal{H} < \frac{\mathcal{F}}{1 - e^{-\mathcal{F}}} \\ \exp \left[ \frac{2\mathcal{F}}{M} + \frac{2(M-1)}{M} \ln \left( \frac{\mathcal{H}}{\mathcal{H} - \mathcal{F}} \right) \right] & \text{if } \mathcal{H} > \frac{\mathcal{F}}{1 - e^{-\mathcal{F}}} \end{cases}. \quad (3.11)$$

Given a value of  $\mathcal{H}$ , we can determine the critical value of  $\mathcal{F}$  that represents the boundary between the two functional forms in (3.11). This can be obtained by solving  $\mathcal{H} = g(\mathcal{F}) \equiv \mathcal{F}/(1 - e^{-\mathcal{F}})$ . We note that  $g \rightarrow 1$  as  $\mathcal{F} \rightarrow 0$  and  $g$  is a monotonically increasing function of  $\mathcal{F} > 0$ . So if  $\mathcal{H} \leq 1$ , then  $D_r$  will be a monotonically increasing function, given by the first line of (3.11).

If  $\mathcal{H} > 1$ , then  $D_r$  is determined by the first line of (3.11) for  $\mathcal{F}$  in the range  $\mathcal{F} \geq g^{-1}(\mathcal{H})$  and by the second line of (3.11) for  $\mathcal{F}$  in the range  $0 < \mathcal{F} < g^{-1}(\mathcal{H})$ . The expression in the second line of (3.11) has a local maximum at  $\mathcal{F} = \mathcal{H} - 1 + M$ , is monotonically

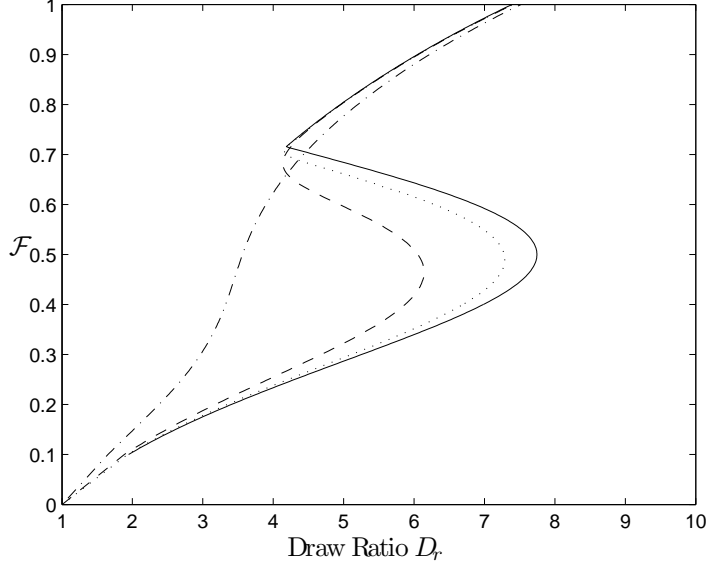


FIGURE 4. The dimensionless force  $\mathcal{F}$  as a function of the draw ratio  $D_r$  for different values of  $K$  for viscosity law (2.7). We have chosen the values for  $M = 0.1$  and  $\mathcal{H} = 1.4$ . The solid line represents the large  $K$  asymptotic limit while the dot-dashed, dashed, and dotted lines are for  $K = 10, 50$ , and  $200$ , respectively.

increasing for  $\mathcal{F} < \mathcal{H} - 1 + M$ , and monotonically decreasing for  $\mathcal{F} > \mathcal{H} - 1 + M$ . If the location of this maximum is in the range  $0 < \mathcal{F} < g^{-1}(\mathcal{H})$ , then  $D_r$  will have a local maximum at  $\mathcal{F} = \mathcal{H} - 1 + M$  and a local minimum at  $g^{-1}(\mathcal{H})$  (shown by the solid line in Figure 4); otherwise  $D_r$  will be a monotonic function of  $\mathcal{F}$ . In Figure 4, we also plot the results for finite values of  $K$  for comparison. We note that in the large  $K$  limit, the local minimum is a corner when the transition layer is ignored. When the transition layer is included, the corner is smoothed out by a small  $O(1/K)$  correction. After some calculation, one can show that the local expansion near the corner is given by

$$D_r = \exp[2g^{-1}(\mathcal{H})] \left[ 1 + \frac{2}{K} (\mathcal{F}_1 + \nu) \right] \quad (3.12)$$

where

$$\nu = \frac{1-M}{M} \{ \exp[g^{-1}(\mathcal{H})] - 1 \} \ln\{1 + M \exp(-2\lambda)\mathcal{F}_1\}$$

and

$$\mathcal{F} = g^{-1}(\mathcal{H}) + K^{-1}\mathcal{F}_1, \quad \lambda = \frac{1}{g^{-1}(\mathcal{H})} - \frac{1}{\exp(g^{-1}(\mathcal{H})) - 1}.$$

The smallest value of  $\mathcal{H} \equiv \mathcal{H}_{min}$  for which  $D_r$  is a non-monotonic function of  $\mathcal{F}$  can be determined by calculating the value of  $\mathcal{H}$  for which the local minimum and local maximum coincide. This can be obtained by solving  $\mathcal{H}e^{-\mathcal{H}} = (1-M)e^{-(1-M)}$ . Since  $\mathcal{H} > 1$  and  $(1-M) < 1$ , this equality can be solved to yield

$$\mathcal{H}_{min} = -W_{-1}[(M-1)e^{M-1}] \quad (3.13)$$

where  $W_{-1}$  is the Lambert-W function (Corless *et al.* 1996) which solves  $W[z]e^{W[z]} = z$ .

In Figure 5, we plot the results of a numerical computation to determine the smallest

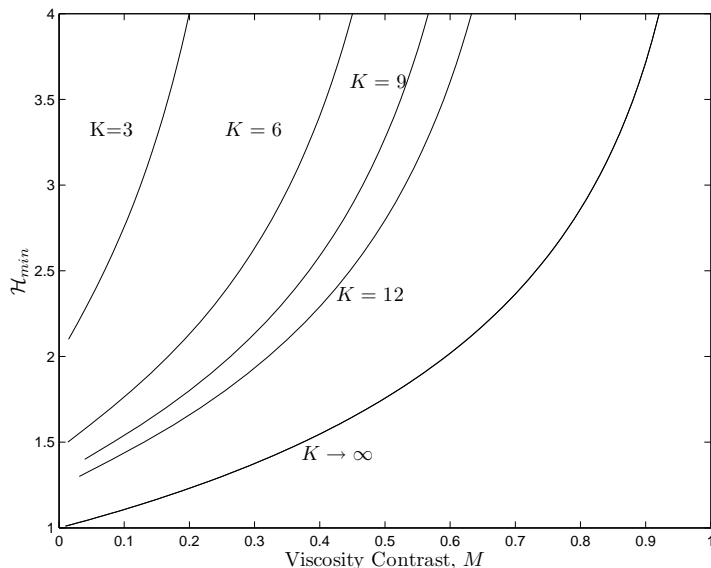


FIGURE 5. The minimum dimensionless heating rate  $\mathcal{H}_{min}$  required to give multiple solutions is plotted as a function of the viscosity contrast  $M$  for different values of the abruptness of the change in the viscosity  $K$ .

dimensionless heating rate  $\mathcal{H}$  that will give rise to the multiple solutions as a function of the viscosity contrast  $M$  for various values of  $K$  and compare with the asymptotic solution for  $K \rightarrow \infty$ . For slowly varying viscosity laws (small  $K$ ) or for viscosity laws that have small absolute changes in viscosity ( $M$  close to unity), the non-unique behavior does not appear even for very large heating rates. However, non-unique behavior can still be achieved for less abruptly varying viscosity laws by localizing the heating. If the heating is applied only over a region of the thread near the device exit at  $x = 1$ , then non-unique behavior appears more readily. This is because the viscosity is constant before entering the heater, but can decrease rapidly in the heater region. This effectively makes the viscosity change much more abruptly.

#### 4. Stability

Fold points similar to those labeled c and d in Figure 2 have been observed in a diverse range of physical problems (Whitehead & Helfrich 1991, Whitehead 1995, Wylie & Lister 1995) closely related to the one studied here. Results from bifurcation theory imply that, generically, the solutions that correspond to these fold points must have a real zero eigenvalue (see for example, Guckenheimer & Holmes 1983, section 3.4 or Iooss & Joseph 1980, section II.8). In examples in which the eigenvalues are always real (Whitehead 1995), this implies that the only changes in stability that can occur are at the two fold points. In most typical cases, the branch connecting the two fold points will be unstable and the other two branches will be stable. However, isothermal thread drawing (for which there are no fold points) has complex eigenvalues and is subject to oscillatory instabilities. Thus one should not expect the eigenvalues for the non-isothermal case to necessarily be real. Although the constraint that there must be a real zero eigenvalue

at the fold points still holds, we will show that other Hopf bifurcations can occur that make the bifurcation structure much more complicated.

In order to investigate the stability of the steady states obtained and described above, we introduce small perturbations of the form

$$A = \hat{A}(x) + \tilde{A}(x)e^{\lambda t}, \quad u = \hat{u}(x) + \tilde{u}(x)e^{\lambda t}, \quad \theta = \hat{\theta}(x) + \tilde{\theta}(x)e^{\lambda t} \quad (4.1)$$

where the steady states are designated with hats and the perturbation quantities with tildes. The quantity,  $\lambda$ , is the growth rate of the perturbations. After substitution of (4.1) into (2.20)–(2.22) and linearization, we obtain the eigenvalue problem

$$\lambda \tilde{A} + (\hat{u} \tilde{A} + \tilde{u} \hat{A})_x = 0, \quad (4.2)$$

$$\left[ \mu(\hat{\theta}) \hat{A} \tilde{u}_x + \mu(\tilde{\theta}) \tilde{A} \hat{u}_x + \mu'(\hat{\theta}) \tilde{\theta} \hat{A} \hat{u}_x \right]_x = 0, \quad (4.3)$$

$$\lambda \theta + \hat{u} \tilde{\theta}_x + \tilde{u} \hat{\theta}_x = -\frac{1}{2} \mathcal{H} \hat{A}^{-3/2} \tilde{A}, \quad (4.4)$$

where  $\mu'$  is the gradient of the viscosity with respect to temperature. The boundary conditions are

$$\tilde{u} = 0, \quad \tilde{A} = 0, \quad \tilde{\theta} = 0 \quad \text{at } x = 0, \quad \text{and} \quad \tilde{u} = 0 \quad \text{at } x = 1. \quad (4.5)$$

This eigenvalue problem was solved numerically by discretizing the equations using up-winding to approximate the spatial gradients and computing the eigenvalues of the resulting matrix. We also verified the results using a complex-valued shooting technique. We will show results for the linear stability as the heating rate increases and non-unique steady states develop.

The natural way to present the results is to plot the real parts of the eigenvalues as functions of the draw ratio,  $D_r$ . However, this is problematic because there can be three possible steady states for a given draw ratio and determining which of the curves corresponds to which basic state can be confusing. In Figure 6, we therefore plot the real parts of the eigenvalues against the dimensionless force,  $\mathcal{F}$ , for a given  $\mathcal{H}$  since there is a one-to-one correspondence between steady states and values of  $\mathcal{F}$ . Nevertheless, it is important to bear in mind that  $D_r$ , and not  $\mathcal{F}$ , is given exogenously. Therefore, one should use Figure 6 in conjunction with Figure 2. This is especially true in the cases where more than one steady state solution exists for a given draw ratio, Figures 6D and 6E. In the most complicated case, Figure 6D, we have labeled various special points for easy comparison with Figure 2.

We plot the real parts of the two eigenvalues with largest real parts as functions of  $\mathcal{F}$  for various values of  $\mathcal{H}$  with a viscosity law that varies abruptly with temperature (large  $K$ ). In Figure 6A, we show the stability results for the unheated case,  $\mathcal{H} = 0$ . In this case, the two eigenvalues with largest real part always form a complex conjugate pair, and so they appear as a single curve. The real part of the eigenvalues increases monotonically with both force and draw ratio until at a critical draw ratio, the real part of the eigenvalues becomes positive, and the solution becomes unstable. This instability is the well-known draw resonance (Denn 1980).

In Figures 6B–D, we see that a critical draw ratio at which the transition from stable to unstable solutions occurs also is present and is only weakly affected by heating. Steady state solutions at these relatively large draw ratios correspond to threads that rapidly move through the device, thus absorbing relatively little heat. This means that the solution will be close to the constant viscosity case, and hence the stability boundary will be similar to that for isothermal drawing.

As the heating rate increases, a number of qualitative changes occur in these graphs,

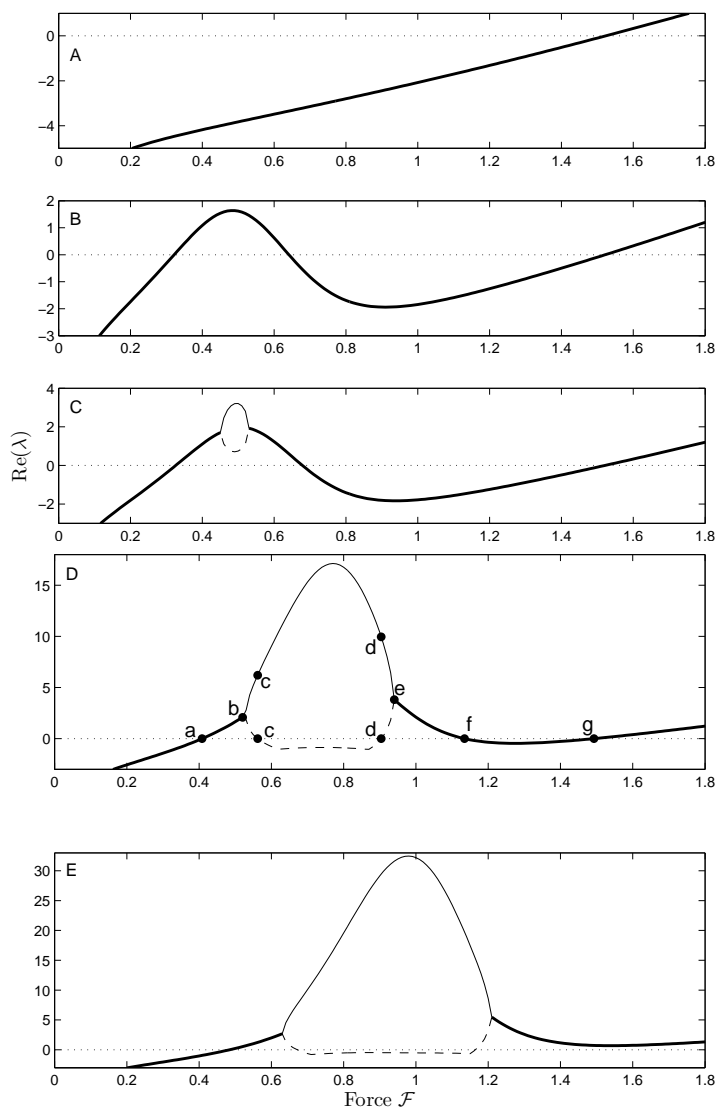


FIGURE 6. The real parts of the most unstable (solid line) and the second most unstable (dashed line) eigenvalues are plotted against the dimensionless force  $\mathcal{F}$  for the five constant  $\mathcal{H}$  curves in Figure 2. When the two eigenvalues form a complex conjugate pair, then the two curves appear as a single bold line. The parameters for the viscosity function are  $M = 0.1$ , and  $K = 12$  and the heating rate takes values  $\mathcal{H} = 0, 1.4, 1.415, 1.6$ , and  $1.75$ . Note that for forces between the points  $c$  and  $d$ , there are three possible steady states for a given draw ratio  $D_r$ . The labels a–g in Figure 6D are provided to allow easy comparison with the  $\mathcal{H} = 1.6$  curve in Figure 2.

and we describe the incremental changes in the following paragraphs. We consider a heating rate  $\mathcal{H} = 1.4$  (see Figure 6B) that is sufficiently small that the required force is still a monotonic function of the draw ratio. The eigenvalues still form a complex-conjugate pair, but the real parts of the eigenvalues become positive in a small window of forces (and hence draw ratios), and the solution will be oscillatorily unstable. This small window exists for draw ratios in the vicinity of the point where the gradient  $d\mathcal{F}/dD_r$  is largest.

For a slightly larger heating rate of  $\mathcal{H} = 1.415$ , the required force is still a monotonic function of the draw ratio. The results are shown in Figure 6C. There is still a small window of instability, but in a portion of this window, the two eigenvalues are not a complex-conjugate pair. As the force increases, these eigenvalues collide on the positive real axis of the complex eigenvalue plane and then separate and move along the positive real axis. The eigenvalues then return and collide again and move off the real axis into the complex plane as a complex-conjugate pair. Therefore, inside the small window of instability, there is an even smaller window in which small disturbances will initially grow without oscillating.

In Figure 6D, we consider a value of  $\mathcal{H} = 1.6$  that is sufficiently large for the fold points,  $c$  and  $d$ , to appear in the force-draw ratio graph. The graph of eigenvalues against force is similar to Figure 6C. However, in this case, the required force is no longer uniquely determined by the draw ratio. At fold points  $c$  and  $d$ , one of the eigenvalues must pass through zero (Guckenheimer & Holmes 1983). In this case, it is the second eigenvalue that does so and the overall stability is not affected. For values of the force between the points  $c$  and  $d$ , there are three possible solutions. If the eigenvalues were plotted against draw ratio, the part of the graph between  $c$  and  $d$  contains three stability curves. Therefore, the branch in Figure 2 that is below the point  $a$  is stable, the branches between the points  $a$  and  $f$  are unstable, the branch between  $f$  and  $g$  is stable, and the branch beyond the point  $g$  is unstable. Since  $a$  has a smaller draw ratio than  $f$ , there is window of draw ratios in which all three solutions are unstable.

As  $\mathcal{H}$  increases, the region in which non-unique steady states exist becomes larger. For sufficiently large values of  $\mathcal{H}$ , the region with multiple steady states becomes so large that the eigenvalues on the branch from the point  $e$  onwards will not cross the real axis, so the points  $f$  and  $g$  will not exist. This means that only the solutions with forces less than a critical value are stable and all other solutions are unstable. In this case, there is no separate window of instability, and the net effect has been to move the instability boundary to low values of the draw ratio.

In Figure 7, we plot the region of parameter space for which the solution is stable (shaded dark) in the  $\mathcal{F}-\mathcal{H}$  plane. Thus, one can clearly see that as  $\mathcal{H}$  increases from 1.3 to 1.7, a small window of instability develops, grows in size, and eventually merges with the draw resonance boundary. The region in which the force decreases with increasing draw ratio is also shown (shaded light). Even though it is not important for the overall stability, we also plot the boundaries where the instability becomes non-oscillatory (dashed line). For easy comparison with Figures 2 and 6D, we also label the points a–g for  $\mathcal{H} = 1.6$ . In Figure 8, we plot the stability boundary (solid line) in the  $D_r - \mathcal{H}$  plane along with the region in which multiple solutions exist (shaded light). For clarity, in this case, we omit the boundaries where the instability becomes non-oscillatory. One should take particular care when viewing this figure because in the shaded region, there are three possible solutions and, hence, three different manifolds. The two branches of the stability boundary (solid line) are embedded in different parts of the manifold (see Figure 2). Again, we have labeled the point a–g for  $\mathcal{H} = 1.6$ . for easy reference.

Although the behavior shown in Figure 6 illustrates many of the important features that occur in glass drawing, there are a number of possible variations that can occur. Firstly, in Figure 2, the point  $a$  has a lower draw ratio than at the point  $f$ , so there is a small region of draw ratios between  $a$  and  $f$  in which no stable solution exists. On the other hand, for more abrupt viscosity laws, the situation can arise in which the point  $f$  has a lower draw ratio than the point  $a$ , so there exists a small region of draw ratios in which two stable steady states exist.

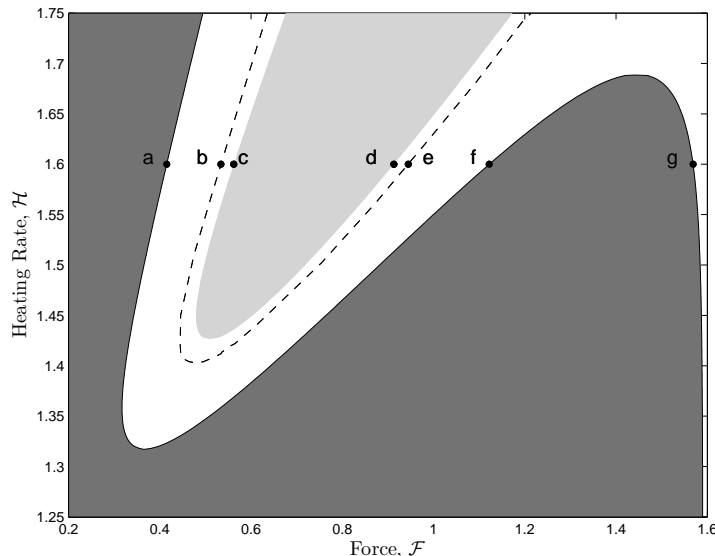


FIGURE 7. The region of parameter space in which the solution is stable (shaded dark) and the region of parameter space in which multiple solutions exist (shaded light) are shown in the  $\mathcal{F} - \mathcal{H}$  plane for a viscosity law with  $M = 0.1$  and  $K = 12$ . For completeness, we also plot the boundary where the two largest eigenvalues are real and equal (dashed line). The points labeled  $a-g$  are included for easy comparison with Figure 6D.

## 5. Conclusion

We have shown that the drawing of viscous threads in the presence of heating can lead to a novel thermo-viscous instability. If the heating is sufficiently strong and the magnitude and abruptness of the viscosity variation are sufficiently large, then three possible steady state solutions can coexist. One of these three steady states has the property that small increases in the draw ratio lead to decreases in the required force and is always unstable. We also have determined the mechanism that underlies the non-uniqueness. We have considered the linear stability of these flows and shown that small windows of stability can arise that are not present in the isothermal case. We hope that this work will motivate further experimental studies, that carefully examine the effects of external heating on draw resonance. In experimental studies, it may prove easier to detect the non-unique steady states by using a fixed pulling force rather than a fixed draw ratio. In this case, the system is hyperbolic and so no absolute instabilities (including draw resonance) will occur. Hence, in principle, one could realize solutions corresponding to all three of the branches.

**Acknowledgment** We wish to thank Drs. Demetrius Papageorgiou, Michael Siegel, Yuan-Nan Young, and Wendy Zhang for useful discussions at the Focused Research Group in Banff. Also, we thank BIRS for funding the FRG and the staff at BIRS for their wonderful efforts to make the FRG such a productive event. This research was supported in part by research grants to HH from the Natural Sciences and Engineering Research Council (NSERC) of Canada and MITACS NCE (Canada), RMM from the Department of Mathematical Sciences, New Jersey Institute of Technology, and JJW was supported by a grant from CityU (Project No. ???).

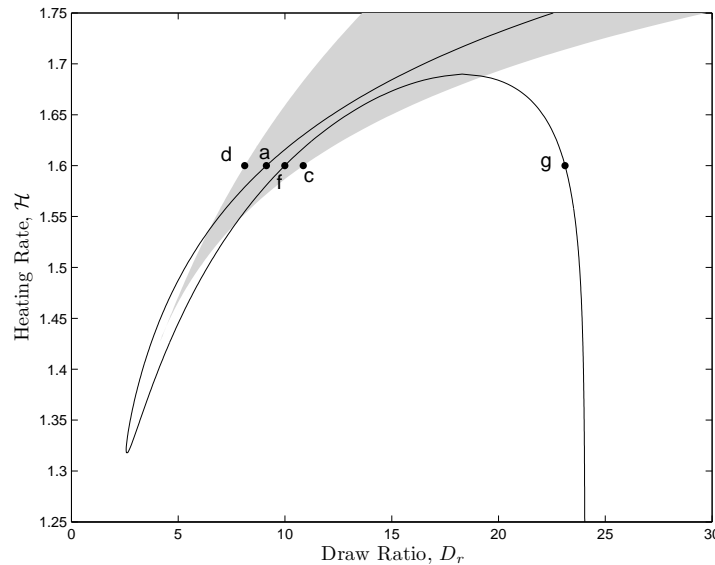


FIGURE 8. The region of parameter space in which multiple solutions exist (shaded light) and the stability boundary (solid line) are plotted in the  $D_r - \mathcal{H}$  plane for a viscosity law with  $M = 0.1$  and  $K = 12$ . Special care should be taken when interpreting the stability boundary because the shaded region contains three solutions. The points labeled  $a-g$  are included for easy comparison with Figure 6D.

## REFERENCES

- BLYLER, L.L. & GIENIEWSKI, C. 1980 Melt spinning and draw resonance studies on a poly( $\alpha$ -methyl styrene/silicone) block compound. *Polym. Engg. Sci.*, **20**, 140–148.
- CORLESS, R.M., GONNET, G.H., HARE, D.E.G., JEFFREY, D.J. & KNUTH, D.E. 1996 On the Lambert W function. *Adv. Comp. Math.*, **5**, 329–359.
- CUMMINGS, L.J. & HOWELL, P.D. 1999 On the evolution of non-axisymmetric viscous fibers with surface tension, inertia and gravity. *J. Fluid Mech.*, **389**, 361–389.
- DENN, M.M. 1980 Continuous drawing of liquids to form fibers. *Ann. Rev. Fluid Mech.*, **12**, 365–387.
- DEWYNNE, J.N., OCKENDON, J.R. & WILMOTT, P. 1992 A systematic derivation of the leading-order equations for extensional flows in slender geometries. *J. Fluid Mech.*, **244**, 323–338.
- FISHER R.J. & DENN M.M. 1977 Mechanics of nonisothermal polymer melt spinning *A.I.C.H.E. J.*, **23**, 23–28.
- FITT, A.D., FURUSAWA, K., MONRO, T.M. & PLEASE, C.P. 2001 Modeling the fabrication of hollow fibers: Capillary drawing. *J. Lightwave Technologies* **19**, 1924–1931.
- FOREST, M.G. & ZHOU, H. 2001 Unsteady analysis of thermal glass fiber drawing processes. *Euro. J. Appl. Math.* **12**, 479–496.
- GUCKENHEIMER, J. & HOLMES, P. 1983 *Nonlinear Oscillations, Dynamical Systems and Bifurcations of Vector Fields*. Springer-Verlag.
- GUPTA, G. & SCHULTZ, W.W. 1998 Non-isothermal flows of Newtonian slender glass fibers. *Int. J. Nonlinear Mech.* **33**, 151–163.
- HAN, C.D. & APTE, S.M. 1979 Studies on melt spinning. VIII. The effects of molecular-structure and cooling conditions on the severity of draw resonance. *J. App. Polym. Sci.*, **24**, 61–87.
- HUANG, H., MIURA, R.M., IRELAND, W. & PUIL, E. 2003 Heat-induced stretching of a glass tube under tension: Application to glass microelectrodes. *SIAM J. Appl. Math.* **63**, 1499–1519.
- Pyrex Glass Code 7740, Material Properties (1987) *Brochure Pyrex B-87*.

- IOOSS, G. & JOSEPH, D.D. 1980 *Elementary Stability and Bifurcation Theory*. Springer-Verlag.
- MATSUMOTO, T. & BOGUE, D.C. 1978 Draw resonance involving rheological transitions. *Polym. Eng. Sci.*, **18**, 564–571.
- PEARSON, J.R.A. & SHAH, Y.T. 1973 Stability analysis of the fibre spinning process. *Trans. Soc. Rheol.* **16**, 519–533.
- SHAH, Y.T. & PEARSON, J.R.A. 1972a On the stability of nonisothermal fibre spinning. *Ind. Eng. Chem. Fundam.* **11**, 145–149.
- SHAH, Y.T. & PEARSON, J.R.A. 1972b On the stability of nonisothermal fibre spinning—general case. *Ind. Eng. Chem. Fundam.* **11**, 150–153.
- VASSILATOS, G., KNOX, B. & FRANKFORT, H. 1985 Dynamics, structure development, and fiber properties in high-speed spinning of polyethylene terephthalate, High Speed Fiber Spinning, A. Ziabicki and H. Kawai, editors, J. Wiley and Sons.
- WHITEHEAD, J.A. 1995 Thermohaline ocean processes and models. *Ann. Rev. Fluid Mech.*, **27**, 89–113.
- WHITEHEAD, J.A. & HELFRICH, K.R. 1991 Instability of flow with temperature-dependent viscosity: A model of magma dynamics. *J. Geophys. Res.*, **96 (B3)**, 4145–4155.
- WYLIE, J.J. & LISTER, J.R. 1995 The effects of temperature-dependent viscosity on flow in a cooled channel with applications to basaltic fissure eruptions. *J. Fluid Mech.*, **305**, 239–261.
- YARIN, A.L. 1986 Effect of heat removal on nonsteady regimes of fiber formation. *J. Eng. Phys.* **50**, 569–575.